www.czasopisma.pan.pl   PAN   www.journals.pan.pl
POLSKA AKADEMIA NAUK

Arch. Metall. Mater. **62** (2017), 3, 1703-1712

M. ŁAZIŃSKA*, T. DUREJKO*#, W. POLKOWSKI*

THE EFFECT OF NANOMETRIC α-Al₂O₃ ADDITION ON STRUCTURE AND MECHANICAL PROPERTIES OF FEAL ALLOYS FABRICATED BY LENS TECHNIQUE

Results of the first principle study on a fabrication of FeAl intermetallic based alloy with an addition of nanometric αAl_2O_3 (n-Al_2O_3) particles by the LENS method and a subsequent characterization of the as received materials' structure and properties, are shown in the present work. A series of samples were manufactured using LENS technique while a control of temperature and the size of melted metal pool.

The presence of ceramics nanoparticles was not directly confirmed by microscopy observations. Neither aluminum nor oxygen content was not elevated in the material with n-Al_2O_3 content. Although, indirect methods revealed influence of n-Al_2O_3 addition on the manufactured elements structure. Analyses of porosity has shown that addition of 2% vol. n-Al_2O_3 significantly decreases this feature (~1%), as compared to the reference material made of pure FeAl intermetallic alloy (~5%). The addition of n-Al_2O_3 causes an increase of grain size in Fe40Al intermetallic alloy. An oxidation resistance has been also improved what was associated to the n-Al_2O_3 addition. Four times lower increase of samples mass was noticed for sample with the n-Al_2O_3 addition as compared to the pure Fe40Al intermetallic alloy.

Keywords: FeAl intermetallic, nano-Al_2O_3 addition, Laser Engineered Net Shaping (LENS)

1. Introduction

Conventional methods for producing alloys (such as casting) have a number of disadvantages: an existence of numerous shrinkage porosity due to wide solidification range, a coarse grained structure affected by slow cooling and a lack of effective nucleation sites, a formation of detrimental brittle intermetallics. Recently, some modifications of the solidification process have been developed in order to overcome aforementioned drawbacks of conventional manufacturing methods [1-3]. These modifications include e.g. an addition of alloying elements or a development of rapid cooling and exogenic processes (e.g. a mechanical vibration, an electromagnetic induction). An addition of nano- and micron-sized particles is a new method for an improvement of mechanical properties of metals and alloys through their microstructure modification [1,3-5]. One of the most important required feature of these modifiers is their good chemical and thermal stability (originating from a high melting temperature). Both simple and complex modifiers may be distinguished. The simple modifiers are the pure alloying elements having a high chemical reactivity, eg. calcium, strontium, barium; while the complex modifiers include alloys or chemical compounds. A nano-modification of metallic alloys leads to an improvement of tensile strength, specific elongation as well as the corrosion and abrasive resistance [3,6-8]. Lazarova et al. [1] reported that nano-modifiers strongly increase the part of the surface energy

in the complete energy balance of the alloy, which determines the phase transformations. On the other hand, the nano-modifiers have a low wettability and they are hardly wetted by a molten material. During an introduction of non-metallic nano- or micron-sized particles to a molten metal, a local overcooling giving proper conditions for a volume crystallization with active crystallization nucleus are obtained [2]. This leads to a significant grain refinement, an alteration of crystal morphology and thus an improvement of mechanical properties of metals and alloys [6].

Carbides, borides, nitrides and oxides nano-particles are usually used as modifiers in order to both improve a microstructure of actually existed cast materials as well as to create a new materials design [1-2,6,10-11]. In practice, the choice of modifiers is related to economic reasons and ease of performing the procedure modification. For example, SiC and Al_2O_3 nanoparticles are used as materials to reinforcement Al alloys due to their relatively good thermal and chemical stability as compared to other types of nano-particles [6,9]. The modification with nano and micron-sized particles has been already successfully performed in e.g. cast iron and steels [1,10], Al alloys [3] or Mg alloys [6]. In recent years intermetallic based alloys from transition metals – aluminum binary systems (e.g. Ni-Al [12-18] or Fe-Al [19-25]), so called aluminides, have gathered a lot of attention from both scientific and industrial environments in terms of their high temperature applications. Fe-Al intermetallic alloys exhibit a high resistance towards oxidation, carbonization

*   MILITARY UNIVERSITY OF TECHNOLOGY, DEPARTMENT OF ADVANCED MATERIALS AND TECHNOLOGIES, 2 KALISKIEGO STR., 00-908 WARSAW, POLAND

Corresponding author: tomasz.durejko@wat.edu.pl

and corrosion at elevated temperature, that make them competitive to conventional high temperature materials. Moreover, these materials combine high yield strength with relatively low density. However, a high brittleness and a low creep resistance above 600°C limit commercial applications of these materials. These drawbacks can be improved in substantial extent by an oxide dispersion strengthening or a grain size refinement [26]. It has been recently shown by few researchers that the addition of nanoceramics e.g. Al_2O_3, Y_2O_3, ZrO_2 is beneficial in terms of high temperature properties (e.g. a creep resistance) of iron based alloy [26-31]. Oxide ceramic particles are relatively inexpensive, chemically inert and do not worsen the oxidation resistance of iron aluminides. However, in contrast to carbides or borides particles, oxide particles are not wetted by liquid iron aluminides what makes it difficult to use them upon the fabrication process [31]. As it has been reported by Zhang et al. [27] and Morris et al. [28] the addition of Y_2O_3 particles improves the creep resistance of Fe–40Al alloy. Similar results has been shown by Subramanian et al. [29] who has suggested that the addition of Al_2O_3 significantly improves the strength properties. The effect of particles addition on properties of Fe-Al alloys is depended on their type, shape, size and distribution in the matrix.

Actually, the Fe-Al alloys with nanoceramics addition are manufactured by various techniques such as a casting, a thermal spraying, a sintering, a self-propagating high-temperature synthesis, a hot-pressing consolidation, etc. [5,13-31,37]. However, these methods are complex, inefficient, energy-consuming and generates high production costs. Moreover, structure of obtained materials is usually characterized by an inhomogeneous distribution of the reinforcement phase in a metal matrix. The drawbacks of aforementioned techniques are driving force for an extensive research on new, advanced manufacturing technologies. A Laser Engineered Net Shaping (LENS[TM]) [32] is a new, promising and innovative method of production of Fe-Al alloys. As compared to other, traditional techniques, the LENS has a few important advantages, such as an easier control of matrix structure and reinforcement particles distribution, a production of near-net shaped components and a possibility of using wide engineering materials range. The process takes place in a protective atmos-

phere in which level of oxygen and water vapour is less than 10 ppm. The LENS systems use laser energy to build up elements directly from metals, alloys, ceramics or composites powders [32-34]. This technology through a layer by layer reproduction of CAD designed project and by using advanced controlling devices allows a precise reconstruction of component geometry. The LENS system is equipped with numerically controlled motors that make possible movement of laser and feed nozzle in the Z-axis and working table in X, Y axis. A powder is injected through four nozzles circumferentially spaced around laser head into a molten pool created by focused, high-powered laser beam, where is melted and deposited on the substrate or previous layer of material. The head is moved up in Z axis with a value equal to the layer thickness and then layer is finished. During the LENS process all technological parameters e.g. a powder feed rate, a laser power and a working table feed are precisely controlled. Additionally, system allows determining a temperature profile of molten pool and then calculating e.g. temperature gradient, cooling rate etc. Additionally, high cooling rates obtained upon the LENS process allows receiving a refined microstructure that can lead to an improvement of mechanical properties [35]. Therefore, the laser-based LENS technique can be considered as an alternative method of production and modification of technologically difficult materials such as Fe-Al intermetallic based alloys.

Results of the first principle study on a fabrication of FeAl intermetallic based alloy with an addition of nanometric αAl_2O_3 (n-Al_2O_3) particles by the LENS method; and a subsequent characterization of the as received materials' structure and properties, are shown in the present work.

2. Experimental details

2.1. Materials

The spherical alloy powder with a nominal composition of Fe40Al0.05Zr-50ppm B (at. %) (LERMPS, France) and a particle size of 44-150 μm was used as an initial powder (Fig. 1a). The small amounts of Zr and B are added to the FeAl alloy in order
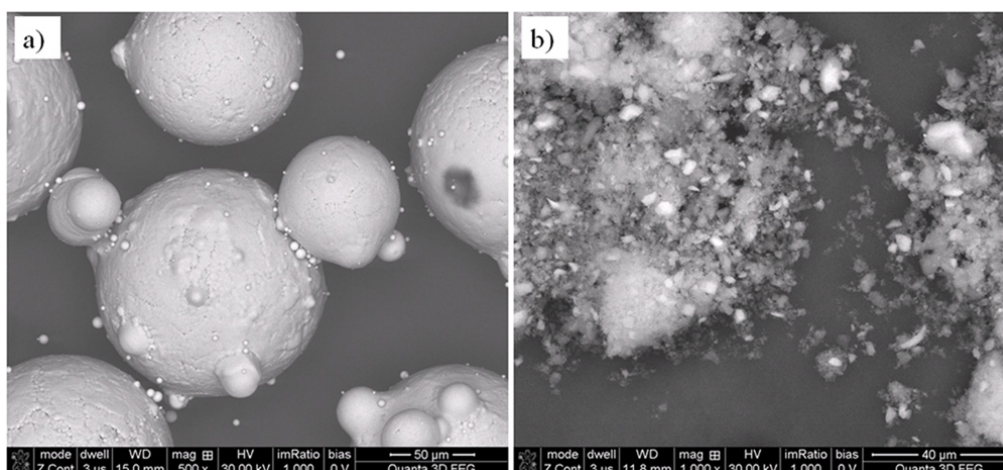

Fig. 1. SEM microphotographs showing a morphology of a) Fe40Al0.05Zr-50ppmB and b) αAl_2O_3 nanoceramic powders

to strengthen a grain boundaries cohesion [36]. Nanometric Al_2O_3 particles (Alfa Aesar GmbH & Co KG) (further referred as n-Al_2O_3) with an average diameter of 35 nm (Fig. 1b) were used as a modifier in the manufacturing process.

2.2. Materials processing

In the first step, the FeAl powder was milled with 2 vol. % of n-Al_2O_3 in a Fritsch PULVERISETTE 7 planetary ball mill with a rotational speed of 200 rpm for 10 minutes. The main objective of the milling process was to obtain an uniform distribution of the ceramic on the surface of the base powder particles, while maintaining the morphology of powder- spherical shape and granulation in the range 44÷150 μm (this particles size of initial powder is required by the LENS technology). The milling parameters were adopted from our previous work [37]. Before milling, a mixture of both powders was prepared inside a glove box in a protective argon atmosphere (H_2O as well as O_2 contents were below 10 ppm). Subsequently, the raw material (about 106 g) was placed in an 80 ml stainless steel bowl with 21 steel grinding balls (with a diameter of 10 mm).

Samples of FeAl without (a reference material) and with n-Al_2O_3 additions were prepared by the LENS MR-7 (300x300x300mm of working area) laboratory system with IPG YLS 500W fiber laser (the emission wavelength is 1070 nm). The laser works in continuous mode. The laser beam spot size have a second-moment diameter of 0.8 mm at the applied working distance (working distance of 9.52 mm was used, as measured from the substrate to four powder nozzles located around the laser head). Energy distribution in the beam is called "top-hat". The polarization of laser beam is random. The process was carried out in strictly controlled atmosphere of argon in which the oxygen content is below 10 ppm. The powder was fed using high-purity argon as a carrier gas, whose flow was 3 l/min. Also, the argon gas was used as a shielding gas to protect the optical lens from powder intrusion and flares.

The system is also equipped with a thermal camera (ThermaViz^{TM}) with a two-wavelength pyrometer and a software designed for temperature recording during a deposition. The long band selected was from 850 nm to 950 nm, and the short band from 750 nm to 850 nm. Cooling rates during a laser surface melting was estimated using the following equation:

$$\frac{dT}{dt} = \frac{VdT}{dx}$$ (1)

where V – a traverse speed [mm/s], dT/dx – a temperature gradient.

The FeAl powder (both with and without n-Al_2O_3) was deposited on a previously sand-blasted surface of Armco iron substrate with thickness of 11 mm in the form of samples with dimensions of 8×8×8 mm. The CAD model is automatically sliced into a tool-path, which instructs the LENS machine how to build the part. The part is constructed layer by layer under the control of software that monitors of parameters. In the first

step, the contour of sample is deposited. Next the head moves to deposition of single paths of the volume (parallel hatches were deposited using a zig-zag system). On each layer, a contour was first deposited along the perimeter of the part, followed by hatches. After the consolidation of one cross-sectional layer, the material deposition head moves on to the next layer which is deposited at an angle of 90 degrees to the previous layer and such process is repeated until a 3D part is completed. The height increment was set as 0.2 mm per layer. Numerically controlled stages allow for the laser and feed nozzles transfer in the Z-axis and movement of the table in X, Y axis, with a positioning accuracy of ±0.25 mm and a linear resolution of ±0.025 mm. Results of a preliminary investigation of samples fabricated under different technological conditions revealed that the best metallurgical quality (represented by the lowest porosity and a lack of cracking) was obtained for following parameters: the laser power – 300W, the traverse speed – 3.9 mm/s and the powder feed rate – 0.16 g/min. For these selected parameters, the FeAl (as a reference material) and the FeAl doped by 2 vol. % of n-Al_2O_3 samples, were prepared. For each variant the temperature profile of melt pool for a middle layer (in a half-height of a sample) was recorded and then gradient temperature and cooling rate were calculated. An exposure time (a measurement time) was 15 milliseconds with 5 second of interval time (average five temperature profiles for each sample were acquired).

2.3. Materials characterization

FEI Quanta 3D field emission gun scanning electron microscope (FEG SEM) with energy dispersive spectroscopy (EDS) and Nikon MA 2000 optical microscope equipped with NIS-Elements BR 3.2 image analyzer was used in order to observe microstructure and determine the chemical composition of material.

Obtained LENS samples were cut by an electrodischarge machining (EDM) device, perpendicularly to the layer deposition direction, and then mechanically ground on SiC papers followed by a mechanical polishing with 3 μm diamond suspensions on STRUERS PLANOPOL 3 machine. A grain morphology was revealed by a chemical etching with 33%-CH_3COOH, 33%-HNO_3, 33%-H_2O and 1%-HF etchant. An equivalent diameter (ECD) and a shape factor α_k were expressed as follows:

$$ECD = \sqrt{\frac{4 \cdot P}{\pi}}$$ (2)

$$\alpha_k = \sqrt{\frac{4 \cdot \pi \cdot P}{\alpha^2}}$$ (3)

where P and O are the surface area and perimeter of tested object, respectively. The grain size and shape factor were measured in three characteristic regions, defined as: near the edge (A) of sample, in the middle part (B) of sample and near the substrate (C).

A Vickers microhardness testing was performed on each sample using SHIMADZU M machine with 100 g load and load-

ing time of 5s. Mechanical properties such as: a yield strength, an ultimate tensile strength, a ductility and a bending strength were evaluated in tensile tests and three-point bending tests. All samples for tensile test were cut off from the LENS fabricated Fe–Al cuboidal shape samples by an electro discharge machining (EDM) device, perpendicular to the deposition direction (specimens with a size of $11\times2.5\times1.5$ mm^3). Samples for three-point bending tests were fabricated using the LENS system as a cuboid of dimensions $25\times6\times3$ mm. For each material composition, five samples were tested. Tests were performed on Instron 8501 universal testing machine under a displacement control condition at the strain rate of 10^{-3} s^{-1} and at room temperature. The surface of the deformed specimens was studied by field emission gun scanning electron microscope (FEG SEM).

A thermogravimetric analysis was carried out on SETA-RAM TG apparatus. Samples with a diameter of 6 mm were heated up with a heating rate of 50 deg/min to temperature of 800°C, and then isothermally annealed for 24 hours. After the end of the process samples were cooled down with a rate of 20 deg/min. The results were shown as a mass gain on unit area of a sample.

3. Results

Analysis of the FeAl particles size revealed that approximately 90% of particles volume fraction was within the range of $44\div150$ μm (Fig. 2). The resulting particle size range is valid for use in the LENS process, which requires spherical powder of $44\div150$ mm range.

The obtained composite powder was characterized by an uniform distribution of Al_2O_3 nanoparticles on the surface of the FeAl particles powder without significant change in their morphology (Fig. 3).
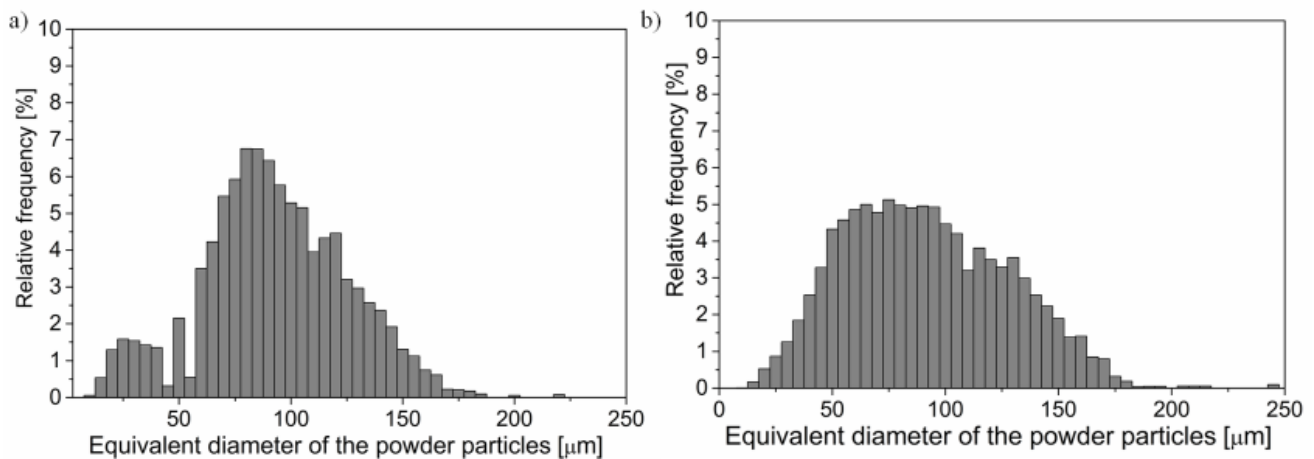

Fig. 2. Particles powder size distributions of a) FeAl and b) FeAl with 2 vol. % of n-Al_2O_3
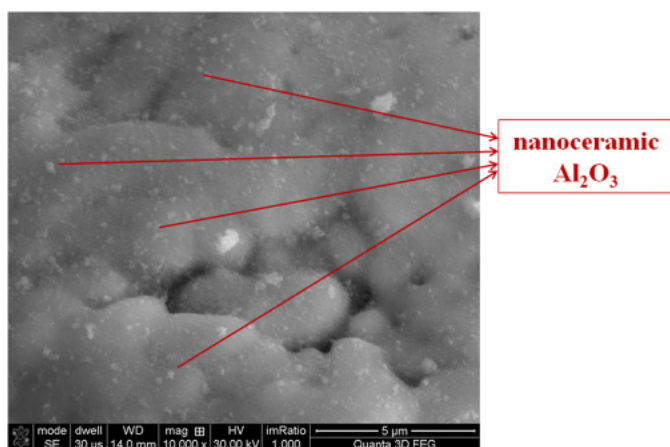

Fig. 3. The FeAl powder after the low-energy milling with 2 vol. % of n-Al_2O_3 ceramic ($t = 10$ min, $n = 200$ rpm)

On the basis of a number of technological tests, it has been found that only samples obtained at a laser power of 300 W, at a traverse speed of 3.9 mm/s and at a powder feed rate of 0.16 g/min have an acceptable metallurgical quality. In other cases, numerous effects of the loss of internal cohesion of the material have been observed, which presumably results from a large thermal stresses. According to reported data [38], in the case of ceramic materials, at a given laser power density, the melt depth is unchanged, while a thermal conductivity significantly decreases. Moreover, ceramic oxide particles exhibit a high absorption of laser radiation, which allows melting under a low laser power. In our process the laser power density (supplied per unit area) was 5.97×10^4 W/cm^2. Upon a laser treatment ceramic particles absorb considerable amount of heat (and thus constitute a barrier to heat flow) leading to some technological problems. Therefore, simultaneous deposition/melting of a powder mixture composed of oxide ceramic and metal is more difficult, due to the extremely different physical properties of constituent components. The FeAl alloy without ceramic addition (the reference material) and the FeAl alloy doped with 2% vol. n-Al_2O_3 were fabricated with the selected parameters.

The microstructure evaluation of the obtained samples was based on microscopic observations, including an assessment of the porosity degree, the grain size and the chemical composition analysis. Obtained results show that the fabricated materials are

characterized by the presence of spherical pores, while the porosity at cross-sections of the samples is approximately five times smaller than in the case of the variant without ceramics. The porosity, as determined using the stereological method, for a sample with the addition of n-Al_2O_3 is 0.8%, while for the reference material (without the addition of n-Al_2O_3) – 5.0%, with a standard deviation equal to, 0.4% and 0.3%, respectively. It is also found that the degree of porosity depends on the area of the sample - the highest porosity fraction is found in the near substrate areas.

Interestingly, the SEM microstructure analysis (Fig. 4), as supported by the results of chemical composition microanalysis (Table 1), did not reveal the presence of nanoceramics particles in the volume of the LENS fabricated materials.

TABLE 1

Results of the EDS chemical composition analysis of FeAl and FeAl with n-Al_2O_3 alloys fabricated by the LENS system

Element	FeAl		FeAl with n-Al_2O_3	
	wt.	at.	wt.	at.
O	0.53	1.45	0.67	1.82
Al	24.90	40.30	24.79	40.03
Zr	0.20	0.07	0.19	0.06
Fe	74.50	58.19	74.50	58.09

The EDS chemical composition analysis carried out for both technological variants confirmed the presence of the FeAl phase (measured content of aluminum and iron is within the FeAl phase area) and trace amounts of zirconium in the alloy structure. In the case of the variant doped with oxide ceramics, an increased oxygen content was reported, as compared to the reference material. A linear analysis of the chemical composition of the observed "second phase" particles revealed the significantly increased intensity of zirconium and a lowered aluminum content in this areas (Fig. 4).

Microscopic observations of etched surfaces of investigated samples revealed the presence of elongated columnar grains (at the substrate), more equiaxed grains in the sample volume and grains very close to equiaxed in the last layers (near the edge of samples), regardless of the analyzed variant (Fig. 5b). The LENS fabrication process is characterized by a presence of high temperature gradient and a high cooling rate which significantly affect the morphology of the resulting microstructure [35,38]. When applying the first layers of a material, a material cooling takes place primarily by theoretically unlimited cold mass in the form of a substrate. This causes a rapid heat dissipation and leads to rapid cooling via the substrate and consequently promotes the directional growth of grains (columnar structure) opposite to the cooling direction. Additionally, the top region of this first layer is the basis for the epitaxial growth of grains in the next deposited layer. When the heat dissipation rate is considerably reduced and the heat transfer through the substrate is no longer dominant, grains with a shape closed to equiaxed appear. In the analyzed cases, a significant deviation from unity for shape factor α_k value was recorded, especially for the area of columnar
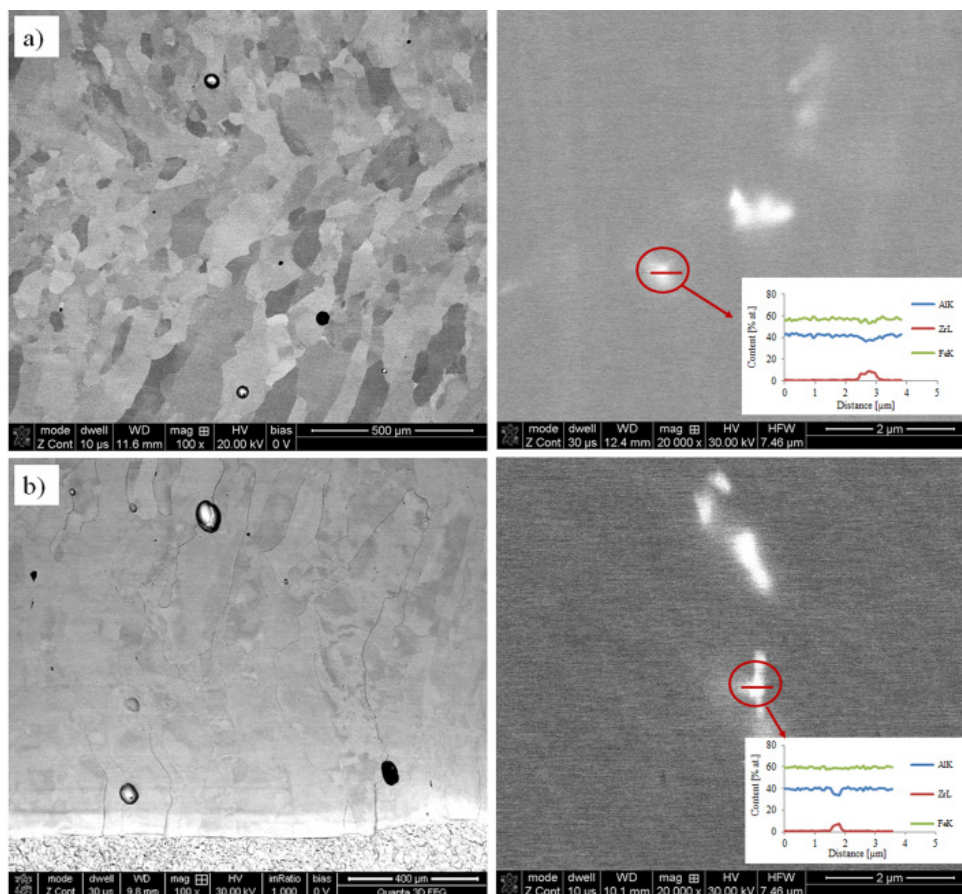

Fig. 4. SEM microphotographs showing microstructural features of a) the FeAl and b) the FeAl with n-Al_2O_3 addition samples

1708

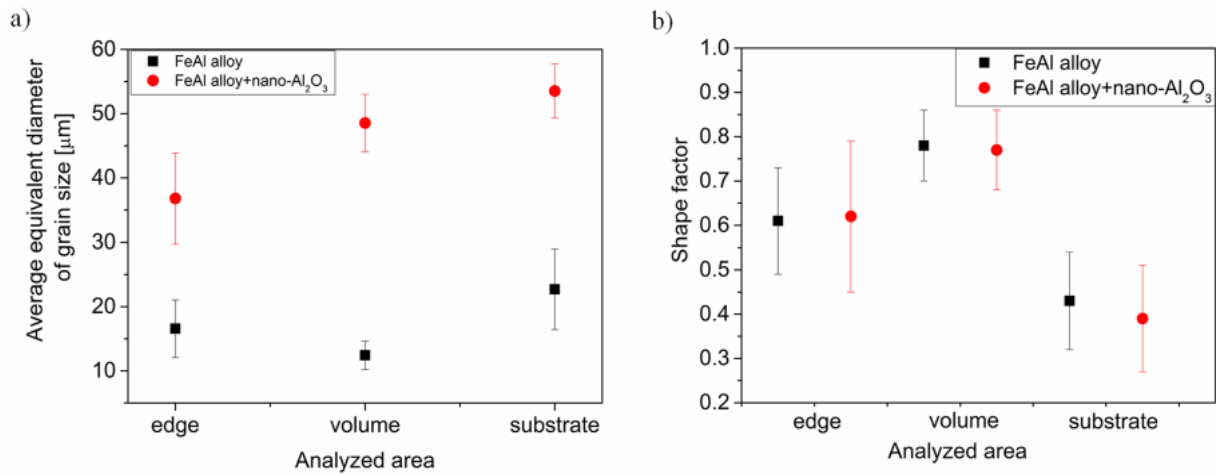Fig. 5. The grain size (a) and the α_k shape factor (b) calculated for a) the FeAl and the FeAl with n-Al$_2$O$_3$ in selected regions (near the top edge of sample, in the middle part – the volume of sample, and near the substrate)

grains. In the near top edge and in the middle part (volume) areas of samples, the microstructure becomes close to the equiaxed structure. Analysis of the α_k factor distributions shows that, at the substrate the mean value fluctuates around 0.4 (Fig. 5b) for both material variants. This indicates that grains at the substrate have a columnar, highly elongated shape. In other areas, grains shape is closed to equiaxed (represented as the α_k factor of 0.6-0.8).

Results of the grain size analysis show that the addition of n-Al$_2$O$_3$ leads to a grain growth of FeAl matrix grains – almost twice higher ECD values were measured. In order to provide a complete statistical analysis of the reference material (without the addition of n-Al$_2$O$_3$) and the material with the addition of nanoceramics, the grain size distribution was represented on histograms for the three specific areas: at the substrate (A), in

the volume (B) and at the edge of the sample (C) (Fig. 6). It is observed that the grain size is different in various sample areas. The effect of grain refinement occurs in the sample edge area. In this region the FeAl alloy with the addition of n-Al$_2$O$_3$ exhibits the largest number of grains within the range of 10-110 µm. In the case of the reference material, the largest fraction of grain fall into the grain size of 10-50 µm. The differentiation of grain size in selected three regions of samples results from the nature of LENS process, and is mainly associated with the directional heat dissipation. For the FeAl + n-Al$_2$O$_3$ alloy grains at the substrate have a diameter of 53 ±5 µm. Similar results were also taken from the middle part of this sample (48 ±7 µm). However, a prominently lower grain size (36 ±8 µm) was observed in the top edge area of the sample with n-Al$_2$O$_3$. In the case of the
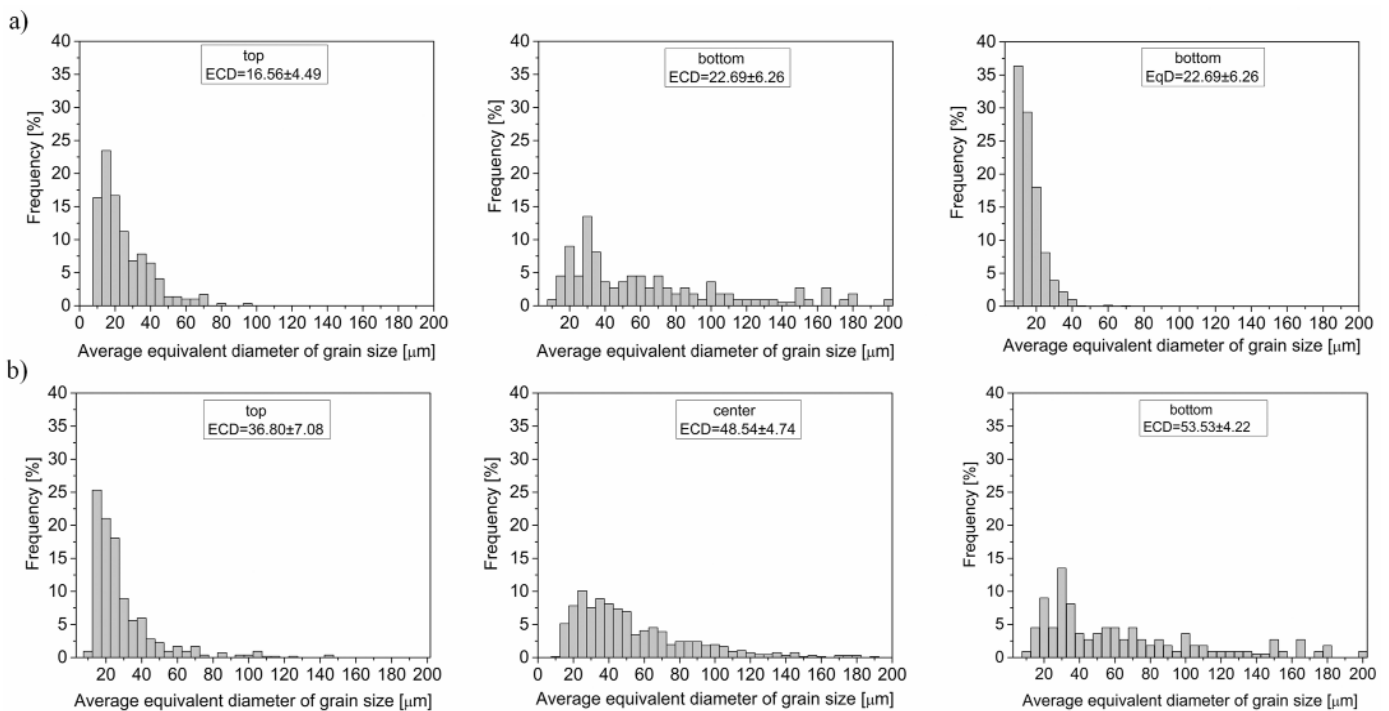

Fig. 6. The grain size distributions obtained from different areas (near the top edge of a sample, in the middle part (center) of a sample, near the substrate (bottom)) of the FeAl, b) the FeAl +n-Al$_2$O$_3$ samples

reference material, average grain size values are smaller and equals 23 ±6 μm, 16 ±4 μm and 12 ±2 μm in the selected areas, respectively (Fig. 6a).

Cross-sectional tests of microhardness were carried out in order to analyze the effect of the n-Al$_2$O$_3$ addition on mechanical properties of the investigated FeAl intrremetallic. Obtained results indicate on a lack of strengthening by the addition of n-Al$_2$O$_3$ to the base material. Both samples exhibit similar hardness, which was even slightly lower for the FeAl + n-Al$_2$O$_3$ than for the "pure" FeAl material (346 ±39 HV0.1 and 322 ±26 HV0.1, respectively. The yield strength $\sigma_{0.2}$, the ultimate tensile strength UTS and the total elongation A_c were received from static tensile tests (Fig. 7).
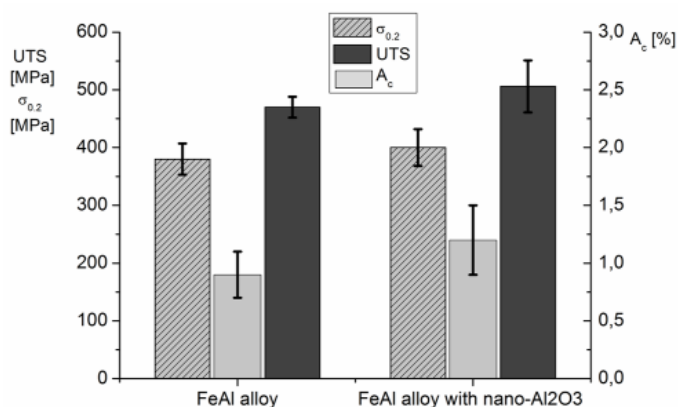

Fig. 7. Mechanical properties of FeAl based alloys with and without n-Al$_2$O$_3$ addition

Based on these results, it was observed that addition of n-Al$_2$O$_3$ causes a small increase in the yield strength and tensile strength, as compared to the reference material (Fig. 7). In the case of both FeAl samples, a similar very low total elongation values were recorded – 0.9% for the pure alloy and 1.2% for the material with n-Al$_2$O$_3$, respectively. It was found that each analyzed sample fail within the plastic deformation regime. However, a SEM fractographic evaluation of fractured surfaces showed the brittle nature of fracture mode (Fig. 8). The photographs show flat, cleavage fracture zones – a so called cleavage facets.

Since the conducted microstructure evaluation did not confirm the presence of n-Al$_2$O$_3$ in the material structure, it was decided to use an indirect method of assessing the possible impact of the ceramic addition on the properties of FeAl alloy. The FeAl intermetallic alloy samples with and without the n-Al$_2$O$_3$ addition were subjected to the thermogravimetric oxidation resistance examination. The kinetic of the oxidation process was analyzed through measurements of sample mass gain per unit area as a function of the annealing time (up to 24 hours) at 800°C, in air. It was observed that, upon the annealing at selected temperature a passive oxide layer appeared on the surface of the tested materials, however its final thickness (after 24h examination) is almost 20 times lower for the n-alumina doped sample than in the case of the pure intermetallic alloy (Fig. 9). Thermogravimetric

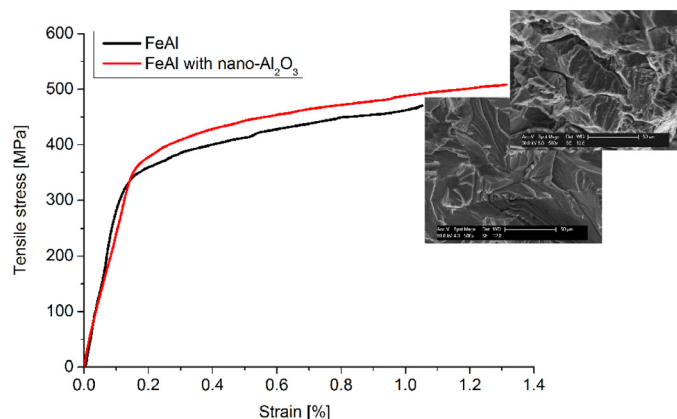Fig. 8. Stress-strain curves and fracture surfaces of FeAl and FeAl+n-Al$_2$O$_3$ ceramic

curves for each variant of the material exhibit two distinctive sections. The initial stage of a rapid oxidation follows with a parabolic course. The parabolic constant of reaction (calculated as $k = \partial^2 \Delta m / \partial t^2$ [mg·mm^{-2}·s^{-1}]) was 8.70×10^{-5} and 1.71×10^{-5} for the pure FeAl sample and the FeAl + n-Al$_2$O$_3$ counterpart, respectively. This shows that the oxidation kinetic is 5-times faster in the pure FeAl as compared to the material with n-Al$_2$O$_3$ addition. The process is continued until the mass gain is completely "saturated", reaching a state of a thermodynamic stabilization represented by a plateau region on thermogravimetric curves. It should be noted that the mass gain is stabilized at a prominently lower level (~0.19 mg/mm^2) for the FeAl + n-Al$_2$O$_3$ specimen than for the pure FeAl (~0.83 mg/mm^2). Moreover, this mass stabilization takes place after a shorter time (12000 s) in n-Al$_2$O$_3$ enriched material than in the undoped sample (17000 s). The absolute final mass gain of the FeAl alloy without the addition of the n-Al$_2$O$_3$ was ~0.13 mg and it was more than 4 times higher than in the case of the material doped with n-Al$_2$O$_3$.

Both materials after the thermogravimetric experiments (annealing at 800°C for 24h under an air atmosphere) were subjected to the linear EDS chemical composition analysis taken on cross sections of specimens. Obtained results point toward
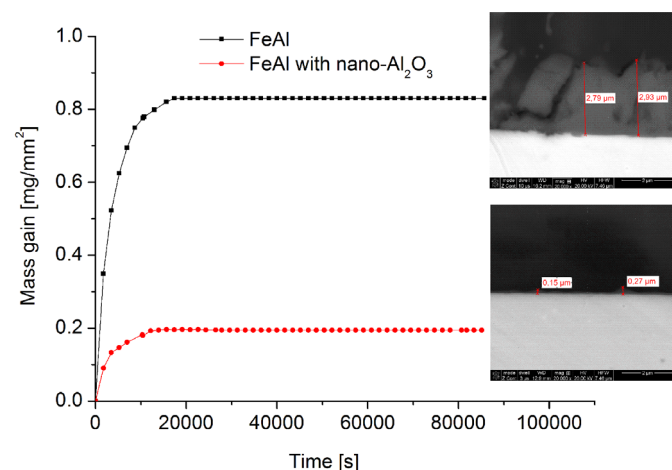

Fig. 9. Mass gain vs. oxidation time plots obtained for the FeAl and FeAl+n-Al$_2$O$_3$ samples

a formation of surface alumina layer in both cases, as evidenced by atomic contents of aluminum and oxygen that correspond to the stoichiometric composition of Al_2O_3 (Fig. 10).

Based on the SEM/EDS evaluation, it was found that the thickness of the resulting surface layer is different in both investigated samples. In the case of the undoped FeAl material, the thickness of the oxide layer was at the level of 3 μm (Fig. 10a), while in the case of the FeAl alloy containing 2% vol. n-Al_2O_3 it was much smaller (0.3 μm) (Fig. 10b). The difference in the analyzed oxide coatings is in a good agreement with results of thermogravimetric tests. Moreover, it was also observed that the oxide surface layer is also much more homogenous in the material with n-Al_2O_3 addition.

An analysis of a temperature distribution in molten pool formed upon the LENS process was carried out in order to clarify the impact of n-Al_2O_3 addition on the FeAl alloy structure. The analysis was conducted by using Thermal Imager device that allows in-situ recording of the temperature distribution of molten pool and thus determination of a number of thermodynamic characteristics. Temperature profiles were determined for individual samples based on results of temperature measurements inside a the molten pool (Fig. 11). During the LENS fabrication of samples with and without the n-Al_2O_3 addition, it was found that the average temperature in the center of the molten pool was slightly higher for the undoped FeAl alloy (2105 ±57°C). In the case of the sample with the addition of n-Al_2O_3 the maximum

recorded temperature was slightly lower (2046 ±35°C). The results indicate that the addition of n-Al_2O_3 leads to increasing of the molten pool area (Fig. 11a), while does not significantly affects its temperature. The calculated molten pool area of the pure sample was 0.95 mm², while in the case of the material with n-Al_2O_3, the surface area was twice larger (2.01 mm²). The addition of oxide ceramics, that exhibit a very low thermal conductivity, increases the heat capacity of the entire material, and thus reduces the heat dissipation rate. As a consequence, the increased volume of the molten pool and a better melting of supplied powder is obtained. The resulting temperature profiles allow determine cooling rates upon the deposition of powders. The addition of n-Al_2O_3 decreases the rate of heat transfer to the "cold" substrate (approx. 6200°C/s on the crystallization front). On the other hand almost 1500°C/s higher cooling rate was recorded for the pure FeAl alloy.

By taking into account the fact that the chemical composition analysis and microscopic observations revealed no occurrence of n-Al_2O_3 particles in the volume of the LENS fabricated material, it was initially assumed that the applied SEM equipment simply does not allow observing ceramic particles due to their very small size. In order to confirm this assumption, additional experiments with a various volumetric content (1, 3 and 6% vol.) of oxide ceramics were conducted.

The process of preparing composite powders and the preparation stage were carried out in the same way as in the case of
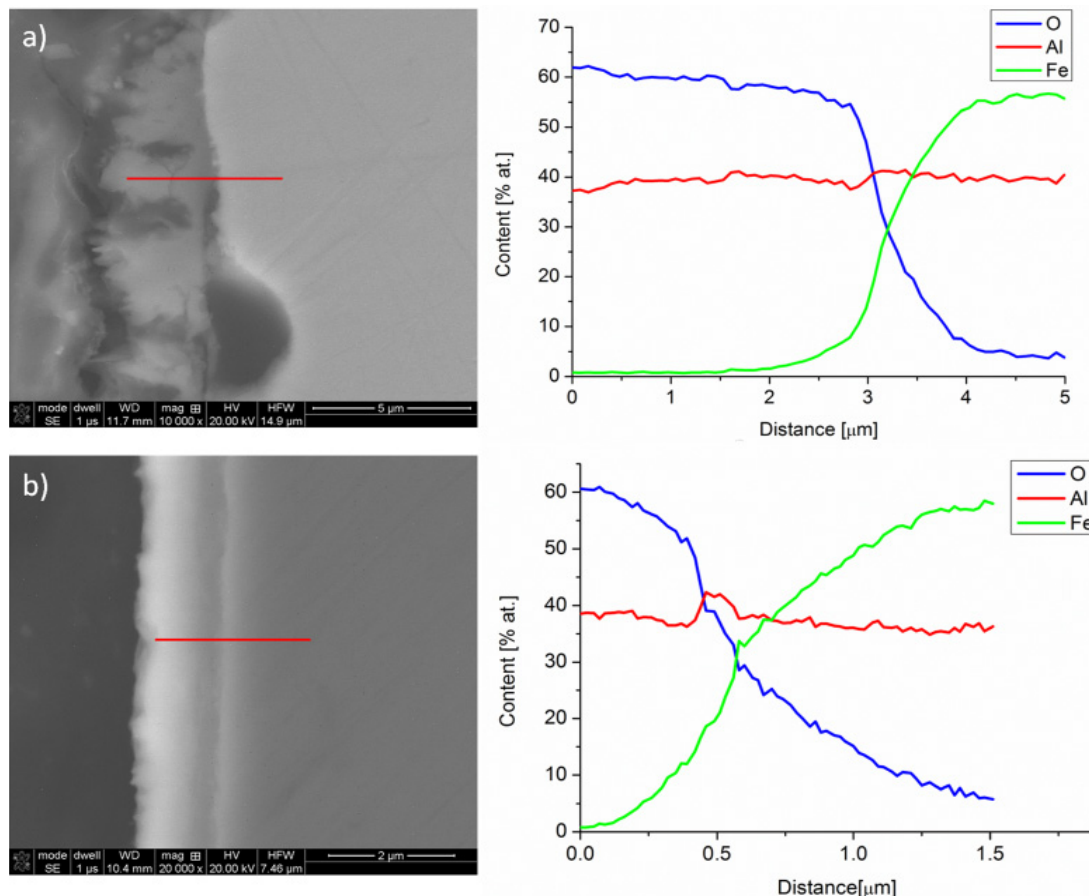

Fig. 10. SEM microphotograps and results of the EDS linear chemical composition analysis after annealing in air for 24h at 800°C: a) FeAl, b) FeAl with n-Al_2O_3
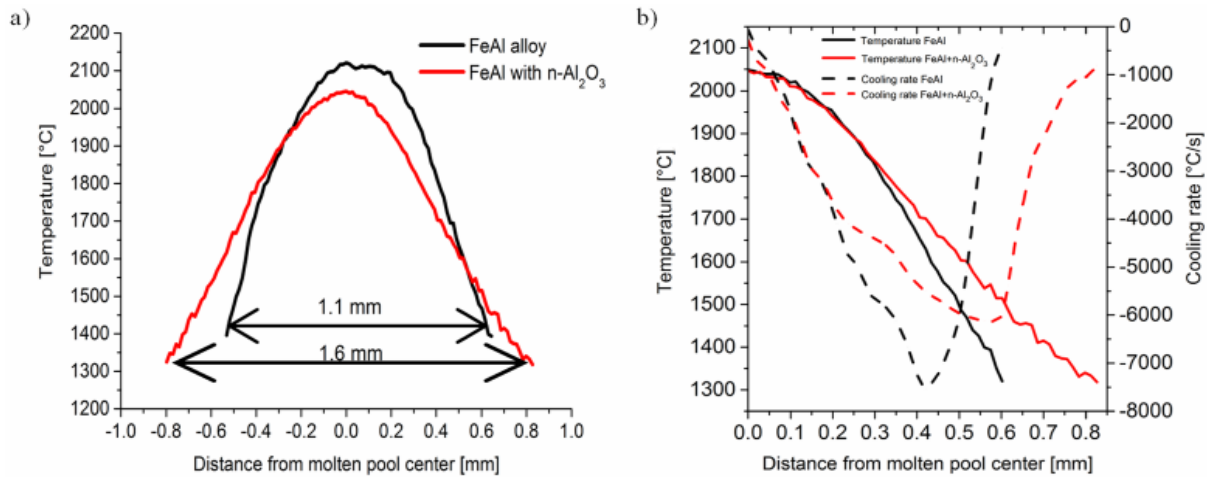
Fig. 11. Thermal Imager profiles of a) temperature, b) gradient temperature and cooling rates of FeAl and FeAl with n-Al$_2$O$_3$ alloys

the previously described FeAl alloy with 2% vol. n-Al$_2$O$_3$. It was found that with increasing nanoceramics content, the geometry of fabricated samples changes and becomes significantly deviated from the assumed geometric model with dimensions of 8×8×8 mm (the height of sample was twice smaller for 6% vol. nanoceramic) (Table 2). Due to the different coefficient of laser radiation absorption of ceramics, its increased content leads to a technological problems upon the LENS fabrication of FeAl intermetallic alloy samples. Moreover, results of conducted structure analysis point towards an increase of a sample porosity with increasing nanoceramic content. Nevertheless, it is worth noted that the porosity of all samples with nanoceramic addition was much lower than that of the reference material (the pure Fe40Al alloy).

Despite of the increased volumetric content of n-Al$_2$O$_3$ addition, the SEM microstructure observations also did not reveal the presence of ceramics in the LENS fabricated material volume. A similar effect was observed by Grosdidier et al. [30] who fabricated Y$_2$O$_3$-doped FeAl alloy by a thermal spraying method. The authors also did not observe the Y$_2$O$_3$ particles within the deposited splats and suggested that the introduced

TABLE 2

Porosity and height samples with different contents of nano-oxide ceramics Al$_2$O$_3$

Sample	Porosity [%]	Height of sample [mm]
Fe40Al+1%vol. Al$_2$O$_3$	1.2	7.59
Fe40Al+2%vol. Al$_2$O$_3$	1.3	7.3
Fe40Al+3%vol. Al$_2$O$_3$	1.8	4.72
Fe40Al+6%vol. Al$_2$O$_3$	2.7	4.14
Fe40Al	5.3	8.62

Y$_2$O$_3$ particles were fractured down to extremely fine size and then are dissolved in the FeAl matrix. The other proposed possibility was that, Y$_2$O$_3$ particles are washed off from the melt due to lack of wetting between the solid Y$_2$O$_3$ and the liquid FeAl. Moreover, since the liquid FeAl does not wet Al$_2$O$_3$ particles a liquid phase assisted sintering of FeAl with Al$_2$O$_3$ ceramic is also problematic. Schneibel et al. [31] suggested that carbides and borides can be better wetted by liquid FeAl as compared to oxide particles. In order to confirm a possibility of the LENS fabrication of materials that are reinforced with nanoparticles, an attempt to produce FeAl alloys containing 2% vol. nano tungsten
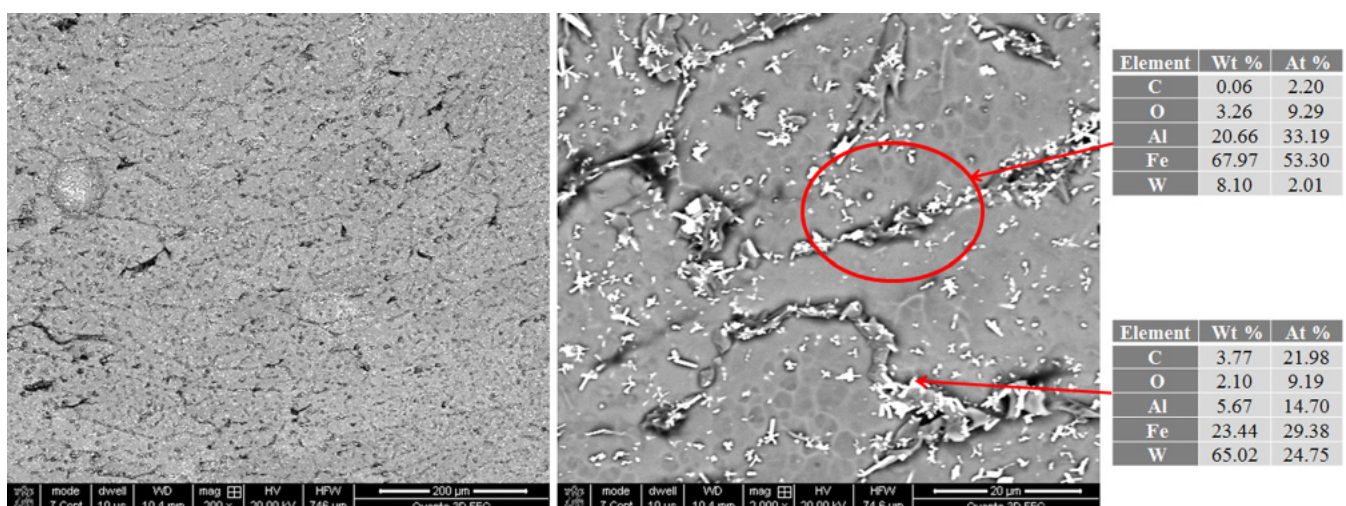

Fig. 12. Microstructure of FeAl with addition of WC

carbide was carried out. All preparation routine and process para-mteres were adopted from the experiments on n-Al$_2$O$_3$ ceramic. In this case, results of the EDS chemical composition and the microstructure observation revealed the presence of carbide in the FeAl alloy matrix (Fig. 12).

4. Conclusions

Based on obtained experimental results supported by proper literature data following conlcusions are listed:

Despite of using a mixture of FeAl alloy and n-Al$_2$O$_3$ powders as a batch material the microstructural evaluation did not reveal a presence of Al$_2$O$_3$ nanoparticles in the LENS fabricated material. Results of mechanical properties analysis show, that the addition of n-Al$_2$O$_3$ does not significantly affect tensile properties of the material. Moreover, it was found that the addition of n-Al$_2$O$_3$ reduces the porosity of fabricated samples and inhibits the grain growth. The most prominent effect of the n-Al$_2$O$_3$ addition was observed upon thermogravimetric tests, where a four times less weight gain per unit area relative to the reference (pure) material, was recorded.

The analysis of temperature distribution during the LENS process shown an increased molten pool area upon the fabrication of the material doped with n-Al$_2$O$_3$. According to results reported in the literature, the addition of oxide ceramics increases the material's heat capacity during laser beam deposition, reduces the heat dissipation rate and thus leading to increase of the molten pool. However, a more thermodynamic analysis of the interaction between FeAl and Al$_2$O$_3$ particles in a molten pool is needed to clarify phase transformations and a structural evolution during the LENS process.

REFERENCES

[1] R. Lazarova, R.H. Petrov, V. Gaydarova, A. Davidkov, A. Alexeev, M. Manchev, V. Manolov, Materials and Design **32**, 2734-2741 (2011).

[2] S.N. Chen, W. Yang, H. Yu, Y.L. Zhang, Journal of Alloys and Compounds **611**, 1-6 (2014).

[3] M. Habibnejad-Korayem, R. Mahmudi, W.J. Poole, Mater. Sci. Eng. A **519**, 198-203 (2009).

[4] C. Senderowski, D. Zasada, T. Durejko, Z. Bojar, Powder Technology **263**, 96-103 (2014).

[5] C. Senderowski, J. of Thermal Spray Tech. **23** (7), 1124-1134 (2014).

[6] H. Choi, H. Konishi, X. Li, Mater. Sci. Eng. A **541**, 159-165 (2012).

[7] S.F. Hassan, M. Gupta, Journal of Alloys and Compounds **429**, 176-183 (2007).

[8] C. Senderowski, M. Chodała, Z. Bojar, Materials **8** (3), 1108-1123 (2015).

[9] A. Mazaherya, H. Abdizadeha, H.R. Baharvandi, Mater Sci Eng A **518**, 61-64 (2009).

[10] Y. Kang, Q. Han, X. Zhao, M. Cai, Materials and Design **44**, 331-339 (2013).

[11] T. Grosdidier, E. Suzon, F. Wagner, Intermetallics **12**, 645-654 (2004).

[12] W. Polkowski, P. Jóźwik, Z. Bojar, Materials Letters **139**, 46-49 (2015).

[13] W. Polkowski, E. Pęczek, D. Zasada, Z. Komorek, Mater. Sci. Eng. A **647**, 170-183 (2015).

[14] W. Polkowski, P. Jóźwik, Z. Bojar, Journal of Alloys and Compounds **614**, 226-233 (2014).

[15] P. Jóźwik, Z. Bojar, J. Bystrzycki, W. Przetakiewicz, Solid State Phenomena **101-102**, 61-64 (2005).

[16] P. Jóźwik, E. Jezierska, Z. Bojar, Materials Chemistry and Physics **81**, 448-451 (2003).

[17] A. Pawłowski, C. Senderowski, Z. Bojar, M. Faryna, Arch. of Metall. and Mater. **55** (4), 1061-1071 (2010).

[18] A. Pawłowski, C. Senderowski, Z. Bojar, J. Bonarski, L. Major, Arch. of Metall. and Mater. **56** (2), 263-269 (2011).

[19] M. Łazińska, T. Durejko, S. Lipiński, W. Polkowski, T. Czujko, R. A. Varin, Mater. Sci. Eng. A **636**, 407-414 (2015).

[20] T. Durejko, M. Ziętala, W. Polkowski, T. Czujko, Materials and Design **63**, 766-774 (2014).

[21] T. Durejko, M. Zietala, M. Łazińska, S. Lipiński, W. Polkowski, T. Czujko, R.A. Varin, Mater. Sci. Eng. A **50**, 374-381 (2016).

[22] T. Durejko, M. Ziętala, Z. Bojar, Materials **8** (2), 575-585 (2015).

[23] A. Pawłowski, C. Senderowski, W. Wołczyński, J. Morgiel, L. Major, Arch. of Metall. and Mater. **56** (1), 71-79 (2011).

[24] A. Pawłowski, T. Czeppe, L. Major, C. Senderowski, Arch. of Metall. and Mater. **54** (3), 783-788 (2009).

[25] W. Wołczyński, C. Senderowski, J. Morgiel, G. Garzel, Arch. of Metall. and Mater. 59 (1), 211-220 (2014).

[26] D.G. Morris, Intermetallics **6**, 753-758 (1998).

[27] W.J. Zhang, R.S. Sundar, S.C. Deevi, Intermetallics **12**, 893-897 (2004).

[28] D.G. Morris, I. Gutierrez-Urrutia, M.A. Munˇoz-Morris, International Journal of Plasticity **24**, 1205-1223 (2008).

[29] R. Subramanian, C.G. McKamey, L.R. Buck, J.H. Schneibel, Mater. Sci. Eng. A**239-240**, 640-646 (1997).

[30] T. Grosdidier, G. Ji, N. Bozzolo, Intermetallics **14**, 715-721 (2006).

[31] J.H. Schneibel, S.C. Deevi, Mater. Sci. Eng. A **364**, 166-170 (2004).

[32] S. Kumar, J.P. Kruth, Materials and Design **31**, 850-856 (2010).

[33] Y. Xiong, J.E. Smugeresky, L. Ajdelsztajn, J.M. Schoenung, Mater. Sci. Eng. A **493**, 361-366 (2008).

[34] Z. Xiaoming, C. Jing, L. Xin, W. Huang, Mater. Sci. Eng. A **478**, 119-124 (2008).

[35] L. Wang, S. Felicelli, Y. Gooroochurn, P.T. Wang, M.F. Horste-meyer, Mater. Sci. Eng. A **474**, 148-156 (2008).

[36] M.A. Munˇoz-Morris, C. Garcia Oca, D.G. Morris, Acta Materialia **50**, 2825-2836 (2002).

[37] T. Durejko, A. Strąk, S. Lipiński, Kompozyty (Composites) **11** (3), 225-229 (2011).

[38] V.K. Balla, S. Bose, A. Bandyopadhyay, International Journal of Applied Ceramic Technology **5**, 234-242 (2008).